HHS Public Access

Author manuscript

Cancer Cell. Author manuscript; available in PMC 2017 April 11.

Published in final edited form as:

Cancer Cell. 2016 April 11; 29(4): 508–522. doi:10.1016/j.ccell.2016.03.002.

Medulloblastoma genotype dictates blood brain barrier phenotype

Timothy N. Phoenix[1], **Deanna M. Patmore**[2], **Scott Boop**[1], **Nidal Boulos**[1], **Megan O. Jacus**[3], **Yogesh T. Patel**[3], **Martine F Roussel**[4], **David Finkelstein**[5], **Lilian Goumnerova**[6], **Sebastien Perreault**[7], **Elizabeth Wadhwa**[6], **Yoon-Jae Cho**[7,8], **Clinton F. Stewart**[3], and **Richard J. Gilbertson**[2]

[1]Department of Developmental Neurobiology, St. Jude Children's Research Hospital, 262 Danny Thomas Place, Memphis, TN 38105, USA [2]CRUK Cambridge Institute, University of Cambridge, Li Ka Shing Centre, Robinson Way, Cambridge CB2 0RE, England [3]Department of Pharmaceutical Sciences, St. Jude Children's Research Hospital, 262 Danny Thomas Place, Memphis, TN 38105, USA [4]Department of Tumor Cell Biology, St. Jude Children's Research Hospital, 262 Danny Thomas Place, Memphis, TN 38105, USA [5]Department of Computational Biology, St. Jude Children's Research Hospital, 262 Danny Thomas Place, Memphis, TN 38105, USA [6]Boston Children's Hospital, 300 Longwood Avenue, Boston, MA, 02115, USA [7]Department of Neurology and Neurological Sciences, Stanford University Medical Center, 1201 Welch Road, Stanford, CA 94305, USA [8]Department of Neurosurgery, Stanford University Medical Center, 1201 Welch Road, Stanford, CA 94305, USA

SUMMARY

The childhood brain tumour medulloblastoma includes four subtypes with very different prognoses. Here, we show that paracrine signals driven by mutant Beta-Catenin in WNT-medulloblastoma – an essentially curable form of the disease – induce an aberrant fenestrated vasculature that permits the accumulation of high levels of intra-tumoural chemotherapy and a robust therapeutic response. In contrast, SHH-medulloblastoma – a less curable disease subtype – contains an intact blood brain barrier, rendering this tumour impermeable and resistant to chemotherapy. The medulloblastoma-endothelial cell paracrine axis can be manipulated *in vivo,* altering chemotherapy permeability and clinical response. Thus, medulloblastoma genotype dictates tumour vessel phenotype, explaining in part the disparate prognoses among medulloblastoma subtypes and suggesting an approach to enhance the chemoresponsiveness of other brain tumours.

Correspondence should be addressed to RJG: Telephone, +44 (0) 1223769590, Richard.Gilbertson@cruk.cam.ac.uk.

Accession numbers

Mouse brain and medulloblastoma endothelial cell RNA microarray data are available from GEO.

AUTHOR CONTRIBUTIONS

Timothy Phoenix conducted the great majority of the studies reported in the paper, including the histology, *in vitro* and *in vivo* mouse work. Deanna Patmore, Nidal Boulos, Megan O. Jacus, Yogesh T. Patel and Clinton F. Stewart completed the preclinical vincristine pharmacokinetic and therapeutic studies. Scott Boop contributed to the histology studies of human and mouse medulloblastoma. Lilian Goumnerova, Sebastien Perreault, Elizabeth Wadhwa, and Yoon-Jae Cho conducted the analysis of tumour inra-operative haemorrhaging in patients treated with medulloblastoma. Richard Gilbertson conceived and supervised the entire research project. All authors participated in the preparation of the manuscript.

INTRODUCTION

Techniques that characterise the sequence and expression of the genome have transformed our understanding of cancer. These approaches are especially powerful for studying tumours that display an important clinical phenotype, such as a dramatic response to treatment (Chang et al., 2014; Marx, 2015). Large-scale sequencing efforts have shown that *TSC1* mutations in bladder cancer, and rearrangements of *ALK* in non-small cell lung cancer, predict response to the mTOR inhibitor everloimus and tyrosine kinase inhibitor crizotinib, respectively (Iyer et al., 2012; Soda et al., 2007; Solomon et al., 2014). Gene expression profiling has also identified subtypes of human cancer that are unusually sensitive to conventional therapies, although the biological reason for this sensitivity is often unknown (Reis-Filho and Pusztai, 2011; Roberts and Mullighan, 2015).

Medulloblastoma, the most common malignant childhood brain tumour, includes four subtypes that are readily identified by genomic profiling (Jones et al., 2012; Northcott et al., 2012b; Pugh et al., 2012; Robinson et al., 2012). SHH-, Group 3- and Group 4-medulloblastomas arise from cerebellar progenitor cells and are fatal in 40% to 70% of cases (Gajjar et al., 2006; Kawauchi et al., 2012; Northcott et al., 2012a; Northcott et al., 2011; Oliver et al., 2005; Uziel et al., 2005; Yang et al., 2008). These tumours contain mutations that activate the SHH pathway (SHH-medulloblastoma) or focal amplifications of *MYC* or *MYCN* (Group-3 and Group-4). In stark contrast, WNT-medulloblastomas arise from the lower rhombic lip, are curable even when metastatic, and frequently contain activating mutations in *CTNNB1* (Ellison et al., 2005; Gajjar et al., 2006; Gibson et al., 2010; Northcott et al., 2012a; Northcott et al., 2011). It is not known if the different origins, driver mutations or some other factor accounts for the different prognoses of medulloblastoma subtypes. Therefore, we sought to understand the biological basis of WNT-medulloblastoma treatment sensitivity since this might improve the treatment of other brain tumours.

RESULTS

WNT-medulloblastomas contain aberrant vascular networks

As a first step to understand the exquisite treatment sensitivity of WNT-medulloblastoma, we looked for features that were unique to these tumours relative to the three other medulloblastoma subtypes. During a comprehensive review of two independent patient cohorts recruited from the Children's Hospital Boston (n=43) and Packard Children's Hospital Stanford (n=45) we found that that 90% (n=9/10) of primary human (h)WNT-medulloblastomas were frankly haemorrhagic at surgery compared with ≤12.5% of the other three subtypes (hSHH-medulloblastoma [12.5%; n=3/24], hGroup 3-medulloblastoma [9%, n=2/22], and hGroup 4-medulloblastoma [0%, n=32]; p<0.0001, Chi-squared; Figure 1A). Remarkably, 60% (n=28/47) of a genetic mouse model of hWNT-medulloblastoma (hereon, mWnt-medulloblasoma) that develops in *Blbp-Cre*$^{+/-}$; *Ctnnb1*$^{+/lox(ex3)}$; *Tp53*$^{+/flx}$ mice also contained macroscopic haemorrhages, relative to only 6.3% (n=2/32) of mShh-medulloblastomas in *Ptch*$^{+/-}$; *Cdkn2c*$^{-/-}$ mice, and 0% (n=0/16) of *Myc*$^{+}$; *Tp53*$^{-/-}$ mGroup 3-medulloblastomas (Gibson et al., 2010; Kawauchi et al., 2012; Uziel et al., 2005;

p<0.0001, Chi-squared; Figure A and B). No mouse model of Group-4 medulloblastoma is currently available.

Because central nervous system (CNS) haemorrhaging can result from aberrant angiogenesis and blood brain barrier (BBB) specification (Vallon et al., 2014), we studied these vascular features in formalin fixed paraffin embedded (FFPE) sections of the different human medulloblastoma subtypes. The mean vascular density of hWNT-medulloblastomas (8.1% ±0.69SE% PECAM1 expression) was approximately four times greater than that of hSHH- (1.9%±0.05SE), hGroup 3- (2.7%±0.30SE) or hGroup 4-medulloblastomas (1.7%±0.42SE; p<0.05, Mann-Whitney; Figures 1 C, D and S1). Immunohistochemical analysis of endothelial cells in these same tumour samples, as well as normal human kidney and brain, showed that hSHH-, hGroup 3- and hGroup 4-medulloblastoma contain $SLC2A1^{+}$/ Plasmalemma Vesicle Associated Protein $(PLVAP)^{-}$ vessels typical of the normal BBB (Daneman et al., 2010a; Stenman et al., 2008). Conversely, hWNT-medulloblastomas contained an aberrant, non-CNS-like, $SLC2A1^{-}/PLVAP^{+}$ vascular endothelium (p<0.001, Mann-Whitney; Figure 1E and F).

To more rigorously quantify the vascular differences among medulloblastoma subtypes, and to determine if these are recapitulated by genetic mouse models of the disease, we used confocal microscopy to measure vessel density (PCAM1 immunoflourescence), tortuosity (number of vessel branch points) and endothelial BBB immunophenotype throughout 50 μm frozen sections of eight variants of genetic mouse models of medulloblastoma. We similarly studied frozen sections of orthotopic xenografts of hWNT- and hSHH-medulloblastoma (hereon, xWNT- and xSHH-medulloblastoma). In keeping with our observations of primary human tumours, all three genetic variants of mWnt-medulloblastoma and xWNT-medulloblastomas contained dense, markedly branched vascular networks that displayed a $Slc2a1^{-}/Plvap^{+}$, non-BBB like immunophenotype (Figures 2A–D and S2). This pattern was significantly different from that seen in the five genetic mouse models of mShh- and mGroup 3-medulloblastoma, as well as xSHH-medulloblastoma that each contained a relatively sparse, non-tortuous and $Slc2a1^{+}/Plvap^{-}$ BBB-like vasculature. Importantly, six of the eight genetic mouse models of medulloblastoma that we studied are generated by Cre-dependent or lentiviral-mediated mutation of neural progenitors and therefore contain wild-type endothelial cells. Thus, although direct perturbation of signaling in endothelial cells can alter BBB development and integrity (Alvarez et al., 2011), vascular phenotype in mouse medulloblastoma appears to be driven by tumour genotype rather than germline mutations inherited by endothelial cells. This is also likely to be true of the great majority of human tumours that rarely arise in the context of germline mutations in WNT, SHH or other signaling pathways.

Medulloblastoma subtypes have different developmental origins (Gibson et al., 2010; Goodrich et al., 1997). Therefore, differences in tumour vessel phenotype could reflect normal regional variations in the developing brain vasculature. To test this, we studied vascular networks in the developing hindbrains of embryonic day (E) 14.5, E17.5, postnatal day (P) 6 and P60 mice. All normal brain regions – including the embryonic dorsal brainstem from which WNT-medulloblastomas arise (Gibson et al., 2010) – contained non-tortuous, $Slc2a1^{+}/Plvap^{-}$ vascular networks similar to those observed in SHH-, Group 3- and

Group 4-medulloblastomas (Figure 2E–H). Thus, the aberrant vasculature of WNT-medulloblastomas is not a developmental legacy. Remarkably, hyperplasia of the embryonic dorsal brainstem that is the precursor lesion of mWnt-medulloblastoma already contained aberrant Slc2a1^{-}/Plvap^{+} blood vessels similar to those found in daughter tumours, while vessels in precursor lesions of mShh-medulloblastomas were morphologically and immunophenotypically normal (Figure 3). Thus, WNT-medulloblastomas possess an aberrant, non-CNS vasculature that is different from the other three disease subtypes and is likely to be driven by tumour genotype.

WNT-medulloblastomas lack a functional BBB

To further characterize the vascular differences among medulloblastoma subtypes we compared the transcriptomes of endothelial cells isolated from normal mouse brains (n=8), mWnt- (n=8 tumours) and mShh-medulloblastomas (n=8 tumours). The transcriptomes of mShh-medulloblastoma endothelial cells were very similar to those of normal brain endothelium (Bolton et al., 1998; Daneman et al., 2010a; Schinkel et al., 1996). In marked contrast, mWnt-medulloblastoma endothelium down-regulated genes normally enriched in CNS endothelium, including Cldn5 and Slc2a1 that are regulated by Wnt signaling in endothelial cells, and upregulated genes expressed in the peripheral endothelium (Figure 4A,B; Zhou et al., 2014). Co-immunofluorescence and/or quantitative reverse transcriptase polymerase chain reaction analyses of a panel of BBB and pan-endothelial markers confirmed these observations (Figure 4 C,D). We also observed down-regulation of several Notch pathway genes in mWnt-medulloblastoma endothelium (Figure 4A). Interaction of Wnt and Notch signaling pathways are known to regulate vascular branching in the developing CNS (Corada et al., 2010), and may partially explain the highly branched phenotype we see in mWnt-medulloblastomas.

Because WNT-medulloblastoma endothelial cells expressed a peripheral vessel-like transcriptome, including PLVAP that is a key component of vascular fenestrations, we looked to see if the vessels in these tumours contained pores (Firth, 2002). As predicted, transmission and 3D scanning electron microscopy readily identified 60–80nm fenestrated pores connecting the luminal and ablumenal compartments of mWnt-medulloblastoma endothelium (Figure 4E). Endothelial tight junctions were also disrupted in mWnt-medulloblastomas, with areas of decreased junctional density and detachment between cells. Conversely, no fenestrations or disrupted tight junctions were observed in mShh-medulloblastoma endothelium (Figure 4F). Vessel coverage by pericytes also plays an important role in BBB maintenance (Armulik et al., 2010; Daneman et al., 2010b; Reis et al., 2012). Pericyte coverage was modestly but significant decreased in mWnt- relative to mShh-medulloblastomas which may be due in part to decreased expression of PDGFβ in mWnt-medulloblastoma endothelium ($p<0.05$, Mann-Whitney; Figure 4A, G).

To test directly if BBB integrity is lost in WNT-medulloblastoma, we measured tumour vessel permeability *in vivo*. The vasculature of normal brain and mShh-medulloblastoma was impervious to systemically delivered 70kDa TMR-Dextran, but TMR-Dextran leaked readily into the tissue fluid of mWnt-medulloblastomas (Figure 5A–C; $p<0.0001$, Mann Whitney). Endogenous immunoglobulin-G also leaked into the tissue fluid of mWnt- but not

mShh-medulloblastomas (Figure 5B). Differences in the extravasation of TMR-Dextran and immunoglobulins were not due to differences in vascular perfusion between tumour subtypes, since intra-vascular levels of systemically delivered Lectin-FITC were similar in mWnt- and mShh-medulloblastomas (Figure 5 B,D). Notably, the hyperplastic precursor lesions of mWnt-, but not mShh-medulloblastoma, were also aberrantly porous (Figure 3). Thus, in contrast to the other medulloblastoma subtypes, WNT-medulloblastomas specify an aberrant, non-CNS vasculature that lacks a functional BBB.

WNT-medulloblastoma paracrine signals block endothelial WNT-signaling

During CNS development Wnt ligands secreted by neural progenitors induce angiogenesis and barriergenesis in neighboring endothelial cells, establishing a paracrine loop that maintains the BBB throughout life (Daneman et al., 2009; Stenman et al., 2008; Ye et al., 2009; Yuen et al., 2014). hWNT- and mWnt-medulloblastomas produce large amounts of WNT antagonists, (e.g. Wnt Inhibitor Factor 1 [WIF1], Dickkopf 1 [DKK1]; Figure 6A,B) presumably as part of a negative feedback loop to silence constitutive mutant CTNNB1 activity (Northcott et al., 2011; Thompson et al., 2006). Therefore, we reasoned that these inhibitors may block WNT signaling and BBB specification in neighboring endothelial cells. As a first step to test this we looked in tumours for evidence of nuclear Lef1 expression that reports active WNT signaling (Logan and Nusse, 2004). As expected, ≥96%±1.2SEM of hWNT, xWNT and mWnt tumour cells in which WNT signaling is constitutively activate, contained $Lef1^+$ nuclei; but ≤23%±2.5SEM of endothelial cell nuclei in these tumours were $Lef1^+$ (Figure 6C,D). The opposite pattern was observed in hSHH, xSHH and mShh-medulloblastomas that contained ≤0.9%±1.7SEM $Lef1^+$ tumour nuclei but ≥82.5%±2.9SEM $Lef1^+$ endothelial cell nuclei (all comparisons $p<0.0005$, Mann-Whitney; Figure 6C,D). Thus, endothelial WNT signaling is markedly reduced in WNT-, relative to SHH-medulloblastoma.

To demonstrate more directly that WNT-medulloblastoma cells secrete factors capable of silencing WNT signaling in adjacent cells, we measured the capacity of tumour cell conditioned media (CM) to suppress enhanced Green Fluorescence Protein (eGFP) expression by a TCF-eGFP reporter cell line (Biechele et al., 2009). mWnt-medulloblastoma cell CM abolished Wnt3a-mediated signaling in this system almost completely, decreasing reporter activity from 89.0%±2.17SEM to 5.6%±1.31SEM ($p<0.0005$ Mann-Whitney; Figure 6E). In contrast, mShh-medulloblastoma CM reduced reporter activity only modestly, from 89.0%±2.17SEM to 72.7%±4.8SEM ($p<0.05$). Changes in phospho-$CTNNB1^{S37/T41}$ expression in reporter cells mirrored the impact of CM on eGFP reporter activity (Figure 6F). WIF1 is one of the most abundant Wnt antagonists secreted by WNT-medulloblastomas (Figure 6A,B). Blockade of Wif1 production by mWnt-medulloblastoma cells significantly impaired the ability of their CM to inhibit Wnt-signaling (Figure 6E and G; $p<0.005$ Mann-Whitney). Thus, paracrine signals from mWnt-medulloblastoma cells that include Wif1 likely silence Wnt-signaling in neighboring endothelial cells.

Disruption of WNT-medulloblastoma paracrine signaling restores the BBB

To test if paracrine signaling between WNT-medulloblastoma and endothelial cells specifies the BBB *in vivo*, we modified the balance of this paracrine loop in tumours. To overcome

the suppressor effect of Wnt inhibitors secreted by mWnt-medulloblastomas, we transduced these cells with a Wnt7a-encoding lentivirus ($mWnt^{Wnt7a}$). Conversely, we generated a Wnt-inhibitory paracrine signal from mShh-medulloblastoma cells by transducing these tumour cells with a Wif1-Dkk1-endcoding lentivirus ($mShh^{Wif1\text{-}Dkk1}$). $mWnt^{Wnt7a}$, $mShh^{Wif1\text{-}Dkk1}$, or empty vector control cells ($mWnt^{control}$ or $mShh^{control}$) were then implanted separately into the hindbrains of CD1-nude mice. Expression of exogenous Wnt7a or Wif1-Dkk1 did not significantly impact medulloblastoma formation or vessel density and tortuosity, although Wnt7a expressing tumour vessels displayed a more tubular morphology (Figures 7A–C and S3). However, secretion of Wnt7a had a profound impact on the vasculature in mWnt-medulloblastomas: restoring almost completely canonical endothelial Wnt signaling ($Lef1^+$ nuclei increase, 21%±22% to 85%±5%; $p<0.005$, Mann-Whitney; Figure 7C,D); reverting the vessel immunophenotype from $Slc2a1^-/Plvap^+$ to $Slc2a1^+/Plvap^-$ (both markers $p<0.0005$, Mann-Whitney; Figure 7 C and E); and generating a functional, TMR-Dextran impervious, BBB ($p<0.005$, Mann-Whitney; Figure 7C and F). Conversely, secretion of Wif1 and Dkk1 by $mShh^{Wif1\text{-}Dkk1}$-medulloblastomas, partially but significantly suppressed endothelial Wnt-signaling ($Lef1^+$ nuclei decrease, 98%±2% to 67%±1%; $p<0.005$, Mann-Whitney; Figure 7C,D) and reverted about a third of vessels from $Slc2a1^+/Plvap^-$ to $Slc2a1^-/Plvap^+$ (both markers $p<0.005$, Mann-Whitney; Figure 7C,E). These relatively modest effects detectably, but non-significantly, increased vessel porosity in $mShh^{Wif1\text{-}Dkk1}$-medulloblastomas (Figure 7C,F).

To further demonstrate the role of tumour-endothelial cell signaling in BBB specification, we generated tumours with admixed populations of $mWnt^{control}$ and $mWnt^{Wnt7a}$ cells. $mWnt^{Wnt7a}$-medulloblastoma cell regions in hybrid tumours contained $Slc2a1^+/Plvap^-$, non-porous, blood vessels, while adjacent $mWnt^{control}$-medulloblastoma regions contained aberrant $Slc2a1^-/Plvap^+$, porous vessels (Figure 7G,H). Thus, tumour-endothelial paracrine signaling dictates vessel phenotype in medulloblastoma and can be manipulated by altering the balance of Wnt agonists and antagonists.

BBB integrity dictates medulloblastoma treatment sensitivity

The BBB impedes the access of chemotherapies to brain tumours (Muldoon et al., 2007). Therefore, we reasoned that the lack of a BBB in WNT-medulloblastomas might increase their exposure to systematic chemotherapy and contribute to the excellent prognosis of these tumours. To test this, we investigated the penetration of systemic chemotherapy into $mWnt^{control}$ and $mShh^{control}$-medulloblastomas *in vivo* and the associated therapeutic response. First, we confirmed that $mWnt^{control}$- and $mShh^{control}$ –medulloblastoma cells are equally sensitive *in vitro* to vincristine, methotrexate and cisplatin that form the backbone of medulloblastoma chemotherapy (Figure 8A). Thus, mWnt-medulloblastomas are not intrinsically more sensitive to chemotherapy. Among these drugs, vincristine has proved especially controversial as a treatment of medulloblastoma since it has limited BBB penetration but causes significant peripheral neurotoxicity (Boyle et al., 2004; Verstappen et al., 2005). Therefore we selected vincristine for further study. Tumour bearing mice were treated with three doses of 1.6mg/kg/dose/week vincristine (equivalent to the clinical dose of $3.3mg/m^2$). Despite the equivalent *in vitro* sensitivity of $mWnt^{control}$ and $mShh^{control}$-medulloblastomas to vincristine, this treatment doubled the median survival time of mice

harboring mWnt^{control}–medulloblastomas but had no impact on the survival of mice with mShh^{control}-medulloblastoma ($p<0.005$, log rank; Figure 8A,B). This difference in treatment response did not correlate with plasma pharmacokinetics that were equivalent between mice harboring mWnt^{control}- and mShh^{control}-medulloblastomas; rather, the tissue fluid of mWnt^{control}-medulloblastomas contained between 30 and 100-fold more vincristine than did mShh^{control}-medulloblastomas, corresponding to a >300 fold increase in tumour distribution coefficient (K_{PT}) of vincristine in mWnt^{control}- relative to mShh^{control}-medulloblastomas ($p<0.05$ for all time points, Mann-Whitney; Figure 8C). Thus, the aberrant vasculature formed in WNT-medulloblastomas by tumour-endothelial cell signaling, renders these tumours porous to systemic chemotherapies that do not penetrate SHH-medulloblastoma, likely contributing at least in part to the excellent prognosis of WNT-medulloblastoma. Finally, as an additional test of this hypothesis we looked to see if the secretion of Wnt7a that restores a functional BBB in mWnt-medulloblastoma without effecting tumour growth, also blocks vincristine efficacy. Although Wnt^{Wnt7a}- and Wnt^{control}-medulloblastoma cells were equally sensitive to vincristine *in vitro,* the restoration of BBB function in Wnt^{Wnt7a}-medulloblastomas blocked access of vincristine to these tumours and rendered them completely resistant to vincristine therapy *in vivo* (Figures 8C,D).

DISCUSSION

Some cancers respond remarkably well to treatment. Better understanding of this treatment sensitivity could identify more effective therapies for less curable tumours (Chang et al., 2014; Marx, 2015). With this in mind, many studies have focused on tumour cell-intrinsic determinants of treatment sensitivity, often seeking mutations that dictate response to small molecule inhibitors of signaling proteins (Iyer et al., 2012; Kool et al., 2014). Much less is known about how the tumour microenvironment influences treatment response; although cancer-associated fibroblasts, immune cells and the vasculature have each been implicated (Junttila and de Sauvage, 2013). For example, colony stimulating factor-1 (CSF-1)-dependent tumour associated macrophages promote the invasion of breast cancer and glioma cells, suggesting CSF-1 as a possible therapeutic target (Pyonteck et al., 2013), and tumour cell-intrinsic WNT signaling has been reported to exclude T-cells from melanoma, promoting resistance to anti-PD-L1/anti-CTLA-4 monoclonal antibody therapy (Spranger et al., 2015). Here, we identify a signaling paradox in which mutant CTNNB1 that drives constitutive, oncogenic WNT signaling in medulloblastoma (Gibson et al., 2010), simultaneously silences WNT signaling in surrounding endothelial cells through the production of secreted inhibitors. As a consequence, WNT-medulloblastomas form a highly aberrant and haemorrhagic vasculature that lacks a BBB, rendering these tumours vulnerable to systemic chemotherapy and potentially explaining why these tumours are curable even when metastatic.

Our identification of differences in the BBB among the various medulloblastoma subtypes has important consequences for the use of existing surgical, radiation and chemotherapies as well as the development of new therapies. Complete resection of medulloblastoma has long been regarded as an important component of curative therapy, but this can result in cerebellar mutism (CM); a devastating syndrome of loss of speech, hypotonia and ataxia (Avula et al., 2015). Therefore, a pre-surgical diagnosis of WNT-medulloblastoma could allow surgeons

to test whether complete resection of these highly curable tumours is required. WNT-medulloblastomas can be differentiated from the other medulloblastoma subtypes using pre-operative magnetic resonance imaging (MRI) because WNT-medulloblastomas arise exclusively from the brainstem (Gibson et al., 2010). However, diagnoses of medulloblastoma subtype that are based on anatomical location alone are inaccurate in one third of patients (Perreault et al., 2014). Our data suggest that the unique vascular phenotype of WNT-medulloblastoma, including the presence of intratumoural bleeding or tumour penetration by BBB-impermeable contrast agents on MRI, could improve the accuracy with which these tumours are diagnosed. Such studies will require the use of large contrast agents that only penetrate a totally compromised BBB, rather than smaller conventional agents e.g., gadolinium (~550Da) that are known to penetrate even a minimally compromised BBB (Perreault et al., 2014).

Radiation is another source of severe long term side effects for survivors of medulloblastoma. Therefore, the excellent prognosis of WNT-medulloblastoma has raised the question of whether these tumours can be cured with minimal or no radiation (Gajjar and Robinson, 2014). While an attractive proposition, ideally the eradication of highly effective radiation therapy would be balanced by the introduction of a new, less toxic curative therapy. But options for these alternative treatments have been limited by the assumption that all medulloblastomas contain an intact BBB that limits drug penetration (Muldoon et al., 2007). Our demonstration that WNT-medulloblastomas lack a BBB suggests a much larger cadre of drugs could be used to treat this tumour; including large molecules such as naked or conjugated therapeutic immunoglobulins. Small molecule inhibitors with limited penetration of an intact BBB should also be considered. For example, the histone deacetylase inhibitor panobinostat is particular attractive since disruption of chromatin modelling is thought play an important role in WNT-medulloblastoma (Northcott et al., 2012a).

In addition to drugs, since the endothelium regulates the traffic of immune cells into tissues, the porosity of WNT-medulloblastoma suggests immunotherapeutic approaches might prove useful to treat these tumours. Indeed, increased vessel patency and porosity have been reported to enhance both immune cell infiltration of tumours and the efficacy of tumour vaccines (Junttila and de Sauvage, 2013). Using these pre-clinical model systems will be important to develop novel combinations of chemotherapeutic regimens that may cure WNT-medulloblastomas without the need for radiation. That said, it is important to note that since the tumour vasculature dictates local the oxygen tension, the aberrant vessels in WNT-medulloblastoma might impact the efficacy of radiation therapy (Jain, 2014). Therefore, testing if the vascular phenotype of WNT-medulloblastoma enhances the radiosensitivity and curability of these tumours will also be important.

Our demonstration that the BBB is intact in SHH-medulloblastoma (and likely the other disease subgroups), underscores the principle that BBB-impermeable drugs are likely to be much less effective treatments of these tumours. Vincristine is a relatively large drug (~825Da), with a high plasma binding affinity, that serves as a substrate for multi drug-resistance transporters; these characteristics markedly impede its ability to cross an intact BBB (Boyle et al., 2004; Wang et al., 2010). Despite these unfavorable pharmacological properties and a toxicity profile that includes severe peripheral neurotoxicity, vincristine is

still used to treat all subtypes of medulloblastoma (Verstappen et al., 2005). We show that mShh-medulloblastomas are impermeable and unresponsive to vincristine *in vivo*, strongly suggesting this drug should not be used to treat this tumour type; a notion supported by studies that have limited the accumulative dose of this drug without impacting survival (Gajjar et al., 2006).

Directly disrupting the BBB in non-WNT-medulloblastomas and other less curable brain tumours might allow the use of otherwise BBB-impermeable drugs to treat these tumours; but, agents that disrupt the BBB have proven difficult to develop (Parrish et al., 2015). In the normal brain, the BBB is maintained by agonistic neuronal-endothelial cell Wnt signaling (Daneman et al., 2009; Stenman et al., 2008; Ye et al., 2009; Yuen et al., 2014; Zhou et al., 2014). We show that an aberrant, antagonistic medulloblastoma-endothelial cell Wnt-signal disrupts the BBB in Wnt-medulloblastomas. Importantly, we also provide proof-of-principle that this paracrine axis can be manipulated *in vivo*. Enhancing Wnt signaling in mWnt-medulloblastoma endothelium restored a functional BBB in these tumours, while secretion of Wnt-inhibitors by mShh-medulloblastomas partially disrupted the BBB. Thus, pharmacological blockade of WNT-signaling in the endothelium of non-WNT-medulloblastoma and other brain tumours might enhance their exposure to systemically delivered therapeutics. Future studies are required to determine the ability of small molecule inhibitors of WNT (Kahn, 2014) to disrupt the BBB and increase chemotherapy penetration in non-WNT-medulloblastomas.

EXPERIMENTAL PROCEDURES

Human tumours

All human data and medulloblastomas were obtained with appropriate informed consent and Institutional Review Board approval. Medulloblastomas were subtyped using Affymetrix gene expression profiling as previously described (Northcott et al., 2011). Surgical reports of patients were reviewed for various clinical features including intra-tumoural haemorrhaging by two independent observers who were blind to medulloblastoma subtype.

Mouse models of medulloblastoma

All animal experiments were performed under St. Jude Children's Research Hospital approved IACUC protocols. mWnt-medulloblastoma ([*Blbp-Cre*$^{+/-}$; *Ctnnb1*$^{+/lox(ex3)}$; *Tp53*$^{+/flx}$; *Pik3ca*$^{loxE545K/loxE545K}$], [*Blbp-Cre*$^{+/-}$, *Ctnnb1*$^{+/lox(ex3)}$; *Tp53*$^{+/flx}$], and [*Blbp-Cre*$^{+/-}$, *Ctnnb1*$^{+/lox(ex3)}$; *Pik3ca*$^{loxE545K/loxE545K}$]), mShh-medulloblastoma ([*Ptch*$^{+/-}$; *Cdkn2c*$^{-/-}$, *Ptch*$^{+/-}$; *Tp53*$^{-/-}$], [*Math1-CreERT2 ; Ptch1*$^{flx/flx}$], and [*hGFAP-Cre*$^{+/-}$; *SmoM2*$^{flx/flx}$]) and mGroup 3-medullobastoma models were generated exactly as described (Gibson et al., 2010; Kawauchi et al., 2012; Uziel et al., 2005). Each of these tumours have been shown to have robust activation of the corresponding Wnt or Shh signal pathway. Mice of the appropriate genotype were subjected to clinical surveillance for evidence of tumour formation as described (Gibson et al., 2010).

cDNAs encoding Wnt7A, Wif1, Dkk1 or empty control were subcloned into the pCDH-EF1-MCS-T2A-copGFP lentiviral plasmid (Systems Bioscience). 19mer shRNA sequences

targeting Wif1: GCTCATAGGATTTGAAGAA, GGGCAGAGATGCATAAATT were cloned into the H1-RFP lentivirus. Orthotopic transplants of tumour cells transduced with control or test lentiviruses were generated exactly as described previously (Mohankumar et al., 2015). Briefly, $1.5x10^6$ tumour cells transduced with a YFP-luciferase lentivirus were resuspended in 5 μl Matrigel an injected via a 3mm borehole into the cerebellum anaesthetised CD-1 nude mice. Mice were monitored for tumour development using bioluminescence (Mohankumar et al., 2015). Medulloblastoma xenografts were similarly generated. One sample each of freshly resected hWNT- and hSHH-medulloblastoma was collected under informed consent with approval of the St. Jude Children's Research Hospital Institutional Review Board. $1.5x10^6$ human tumour cells transduced with a YFP-luciferase lentivirus were then resuspended in 5 μl Matrigel an injected via a 3mm borehole into the cerebellum anaesthetised CD-1 nude mice.

Blood brain barrier permeability and vessel perfusion assays

100 μl of a 10 mg/ml 70kDa Dextran-TMR solution (#D1818, Life Technologies) was injected via the tail vein into mice harboring the indicated medulloblastoma mouse allograft. Two hours later animals were perfused with phosphate buffered saline (PBS) and 4% paraformaldehyde. Their brains were then removed and post-fixed overnight. Vessel perfusion studies were similarly conducted although mice were injected with 1.0 mg/ml Lectin-FITC (Sigma-Aldrich), and brains harvested 10 minutes post injection.

Histology

Tissue microarrays of human tumours were stained immunohistochemically using standard techniques and the following primary antibodies: PECAM1 (1:50; Cell Marque #131M-94), LEF1 (1:250; Cell Signaling #C12A5), SLC2A1 (1:500; Millipore #07-1401) and PLVAP (1:100; Sigma #HPA002279). Dye Light secondary antibodies (488 and 647 conjugates, Jackson ImmunoResearch) were used for fluorescent visualization, along with Hoechst dye (Life Technologies).

Immunofluorescence of 50 μm sections of fresh frozen medulloblastoma mouse allografts or xenografts were performed using standard techniques. Briefly, sections were blocked in 10% normal donkey serum for 1 hour and then incubated overnight with one or more of the following primary antibodies: PECAM1 (1:200; BD Biosciences #550274), LEF1 (1:500; Cell Signaling #C12A5), PLVAP (1:200; BD Biosciences #550563), SLC2A1 (1:1000; Millipore #07-1401), Wif1 (1:500; Abcam #ab33281), Wnt7A (1:500; Abcam #ab100792), PDGFR-β (1:250; eBioscience #14- 1402), Desmin (1:500; Millipore #AB3623), P-Glycoprotein (1:50; Millipore #517310). Sections were then incubated with corresponding secondary antibodies (Jackson ImmunoResearch, Dye Light 488, 594 and 647) and nuclei stained with Hoechst dye (Life Technologies). Sections were imaged using a Zeiss ImagerM2 with Apotome or Zeiss 510 LSM META confocal microscope and analyzed in Axiovision, ZEN, and Image J.

For quantification of vessel density or branch points based on PECAM1 expression or SLC2A1/PLVAP expression, 0.894 μm x 0.670 μm images were collected across serial sections of tumours, and then processed in ImageJ to determine percent area of stain.

PECAM1/LEF1 quantification was performed in ZEN (Zeiss) on random tumor fields at 40 x (0.22 μm2 z- stacks). PECAM1/Desmin quantification was performed on random fields at 20x (0.44 μm2 z-stack). For quantification of TMR-Dextran leakage, entire tumor regions were imaged across serial sections at (0.894 μm x 0.670 μm). GFP^+ tumor regions were selected and TMR pixel intensity recorded for each selection. Human tissue microarray sample cores were imaged in their entirety, and then quantified for blood vessel co-localization of PLVAP/SLC2A1 staining in ZEN.

For electron microscopy (EM) studies, mice harboring mWnt or mShh-medulloblastomas were deeply anaesthetised with Avertin (250 mg/kg) and then perfused with EM buffer (0.1M sodium cacodylate pH 7.4) and fixative (0.1M sodium cacodylate pH 7.4 + 2% Paraformaldehyde + 2.5% Gluteraldehyde). Brains were then and vibratome sectioned into 2% osmium tetroxide in 0.1M cacdylate buffer with 0.15% potassium ferrocyanide, dehydrated and then embedded in epoxy resin. Ultra-thin sections (80nm) were then cut and imaged using a Tecnai TF20 transmitting electron microscope. For 3D scanning electron microscopy, 500 nm thick sections were coated with iridium in a Denton Desk II sputter coater and imaged using a Helios Nanolab 660 FIB-SEM Dualbeam system. 3D image stacks at 5x5x5nm resolution were processed and reconstructed using Amira 6.0 software.

Endothelial cell studies

Tumour and normal brain samples were digested in papain (Worthington, 5 units/ml) and filtered single cell suspensions incubated with mouse Eng-PE and Cdh5-PE antibodies (eBioscences #12-1051, 12- 1441). Cells were then incubated with anti-PE microbeads (Milyenitec) and then processed through two consecutive MS separation columns (Milyenitec). Total RNA was isolated from Eng/Cdh5-PE cell fractions and mRNA expression profiles generated using Affymetrix Mouse Gene 2.0ST microarrays exactly as described (Mohankumar et al., 2015). RNA samples were analysed by reverse transcriptase polymerase chain reaction analysis using the following primers: GAPDH (AGGTCGGTGTGAACGGATTTG; TGTAGACCATGTAGTTGAGGTCA), Pcam1 (ACGCTGGTGCTCTATGCAAG TCAGTTGCTGCCCATTCATCA), Cdh5 (CCACTGCTTTGGGAGCCTT; GGCAGGTAGCATGTTGGGG), Eng (CCCTCTGCCCATTACCCTG; GTAAACGTCACCTCACCCCTT), Slc2a1 (CAGTTCGGCTATAACACTGGTG; GCCCCCGACAGAGAAGATG), Ocln (TTGAAAGTCCACCTCCTTACAGA; CCGGATAAAAAGAGTACGCTGG), Abcb1a (CAGCAGTCAGTGTGCTTACAA; ATGGCTCTTTTATCGGCCTCA), Plvap (GCTGGTACTACCTGCGCTATT; CCTGTGAGGCAGATAGTCCA).

Cell Culture

Primary cultures of mWnt- and mShh-medulloblastoma cells were generated and maintained in Neurobasal medium as described (Gibson et al., 2010). 293T cells transduced with a lentiviral Wnt-reporter construct (Biechele et al., 2009) were treated with Wnt3a (R&D; 120ng/ml) in control or tumour conditioned media for 24 hours before quantifying the proportions of eGFP and mCherry expressing cells by fluorescence activated cell sorting. For western blot analysis, protein lysates were collected from the indicated cells and processed using standard techniques. Blots were probed with the following primary

antibodies: Wif1 (Abcam, #ab33281), Wnt7a (Abcam, #ab100792) β-Actin (Cell Signaling, #4967), Ctnnb1 (Cell Signaling, #9587), phospho-Ctnnb1$^{S37/T41}$ (Millipore, #05-665). Total protein levels were estimated by Coomassie blue staining of nitrocellulose membrane. The proliferation of single cell suspensions of tumour cells cultured in neurobasal medium, in the presence or absence of the indicated drugs was recorded using CellTiter-Glo as described (Atkinson et al., 2011).

In vivo vincristine efficacy and pharmacology studies

For efficacy studies, vincristine was dissolved in 0.9% sodium chloride (0.16mg/ml) and administered via tail vein injection (1.6mg/kg) weekly starting at initiation of tumour growth based on bioluminescence. Mice were imaged for bioluminescence weekly, and monitored daily for neurological symptoms. To define the vincristine disposition in CD-1 nude mice and to derive a pharmacokinetic limited sampling model (LSM), we performed a plasma pharmacokinetic (PK) study in non-tumour bearing CD-1 nude mice. Mice (n=9) were dosed with 1.6mg/kg vincristine and blood samples collected using a population based study design. Each mouse was sampled three times at pre-determined time-points using retro-orbital eye bleeds except at the terminal time-point, where the sample was collected using cardiac puncture. Plasma samples were analyzed using a validated LCMS-MS method and a 2-compartment model was fitted to the plasma concentration-time data using non-linear mixed effect modeling (NONMEM 7.3, ICON Development Solutions, Ellicott City, MD). Two separate tumour disposition studies of vincristine were performed. When mice became symptomatic due to tumour burden, they were dosed with 1.6mg/kg vincristine and sacrificed at LSM derived time-points (5 min, 30 min, and 2 hr) post-dose. Plasma and tumour concentration-time data were analysed using a naïve-pooled analysis. A 2-compartment model consisting of a tumour compartment linked to a central compartment via CLIN (influx clearance) and CLOUT (efflux clearance) was fitted to plasma and tumour concentration-time data using a Bayesian method implemented in ADAPT 5 where PK parameters obtained from the initial plasma PK study were used as priors. The tumour to plasma partition co-efficient (KPT) was calculated as a ratio of area under the tumour concentration-time curve to the plasma concentration-time curve (AUCTumour/AUCPlasma).

Supplementary Material

Refer to Web version on PubMed Central for supplementary material.

Acknowledgments

This work was supported by grants from the National Institutes of Health (R.J.G., P01CA96832 and P30CA021765), the American Lebanese Syrian Associated Charities and Cancer Research UK. We are grateful to the staff of the Hartwell Center for Bioinformatics and Biotechnology, the Cell and Tissue Imaging Shared Resource and the ARC at St Jude Children's Research Hospital for technical assistance.

References

Alvarez JI, Dodelet-Devillers A, Kebir H, Ifergan I, Fabre PJ, Terouz S, Sabbagh M, Wosik K, Bourbonniere L, Bernard M, et al. The Hedgehog pathway promotes blood-brain barrier integrity and CNS immune quiescence. Science. 2011; 334:1727–1731. [PubMed: 22144466]

Armulik A, Genove G, Mae M, Nisancioglu MH, Wallgard E, Niaudet C, He L, Norlin J, Lindblom P, Strittmatter K, et al. Pericytes regulate the blood-brain barrier. Nature. 2010; 468:557–561. [PubMed: 20944627]

Atkinson JM, Shelat AA, Carcaboso AM, Kranenburg TA, Arnold LA, Boulos N, Wright K, Johnson RA, Poppleton H, Mohankumar KM, et al. An integrated in vitro and in vivo high-throughput screen identifies treatment leads for ependymoma. Cancer Cell. 2011; 20:384–399. [PubMed: 21907928]

Avula S, Mallucci C, Kumar R, Pizer B. Posterior fossa syndrome following brain tumour resection: review of pathophysiology and a new hypothesis on its pathogenesis. Child's nervous system : ChNS : official journal of the International Society for Pediatric Neurosurgery. 2015; 31:1859–1867.

Biechele TL, Adams AM, Moon RT. Transcription-based reporters of Wnt/beta-catenin signaling. Cold Spring Harb Protoc. 2009; 2009 pdb prot5223.

Bolton SJ, Anthony DC, Perry VH. Loss of the tight junction proteins occludin and zonula occludens-1 from cerebral vascular endothelium during neutrophil-induced blood-brain barrier breakdown in vivo. Neuroscience. 1998; 86:1245–1257. [PubMed: 9697130]

Boyle FM, Eller SL, Grossman SA. Penetration of intra-arterially administered vincristine in experimental brain tumor. Neuro-oncology. 2004; 6:300–305. [PubMed: 15494097]

Chang DK, Grimmond SM, Evans TR, Biankin AV. Mining the genomes of exceptional responders. Nat Rev Cancer. 2014; 14:291–292. [PubMed: 25688402]

Corada M, Nyqvist D, Orsenigo F, Caprini A, Giampietro C, Taketo MM, Iruela-Arispe ML, Adams RH, Dejana E. The Wnt/β-Catenin Pathway Modulates Vascular Remodeling and Specification by Upregulating Dll4/Notch Signaling. Developmental Cell. 2010; 18:938–949. [PubMed: 20627076]

Daneman R, Agalliu D, Zhou L, Kuhnert F, Kuo CJ, Barres BA. Wnt/beta-catenin signaling is required for CNS, but not non-CNS, angiogenesis. Proceedings of the National Academy of Sciences of the United States of America. 2009; 106:641–646. [PubMed: 19129494]

Daneman R, Zhou L, Agalliu D, Cahoy JD, Kaushal A, Barres BA. The mouse blood-brain barrier transcriptome: a new resource for understanding the development and function of brain endothelial cells. PloS one. 2010a; 5:e13741. [PubMed: 21060791]

Daneman R, Zhou L, Kebede AA, Barres BA. Pericytes are required for blood-brain barrier integrity during embryogenesis. Nature. 2010b; 468:562–566. [PubMed: 20944625]

Ellison DW, Onilude OE, Lindsey JC, Lusher ME, Weston CL, Taylor RE, Pearson AD, Clifford SC. beta-Catenin status predicts a favorable outcome in childhood medulloblastoma: the United Kingdom Children's Cancer Study Group Brain Tumour Committee. J Clin Oncol. 2005; 23:7951–7957. [PubMed: 16258095]

Firth JA. Endothelial barriers: from hypothetical pores to membrane proteins. J Anat. 2002; 200:541–548. [PubMed: 12162722]

Gajjar A, Chintagumpala M, Ashley D, Kellie S, Kun LE, Merchant TE, Woo S, Wheeler G, Ahern V, Krasin MJ, et al. Risk-adapted craniospinal radiotherapy followed by high-dose chemotherapy and stem-cell rescue in children with newly diagnosed medulloblastoma (St Jude Medulloblastoma-96): long-term results from a prospective, multicentre trial. Lancet Oncol. 2006; 7:813–820. [PubMed: 17012043]

Gajjar AJ, Robinson GW. Medulloblastoma[mdash]translating discoveries from the bench to the bedside. Nat Rev Clin Oncol. 2014; 11:714–722. [PubMed: 25348790]

Gibson P, Tong Y, Robinson G, Thompson MC, Currle DS, Eden C, Kranenburg TA, Hogg T, Poppleton H, Martin J, et al. Subtypes of medulloblastoma have distinct developmental origins. Nature. 2010; 468:1095–1099. [PubMed: 21150899]

Goodrich LV, Milenkovic L, Higgins KM, Scott MP. Altered neural cell fates and medulloblastoma in mouse patched mutants. Science. 1997; 277:1109–1113. [PubMed: 9262482]

Iyer G, Hanrahan AJ, Milowsky MI, Al-Ahmadie H, Scott SN, Janakiraman M, Pirun M, Sander C, Socci ND, Ostrovnaya I, et al. Genome sequencing identifies a basis for everolimus sensitivity. Science. 2012; 338:221. [PubMed: 22923433]

Jain, Rakesh K. Antiangiogenesis Strategies Revisited: From Starving Tumors to Alleviating Hypoxia. Cancer Cell. 2014; 26:605–622. [PubMed: 25517747]

Jones DTW, Jager N, Kool M, Zichner T, Hutter B, Sultan M, Cho YJ, Pugh TJ, Hovestadt V, Stutz AM, et al. Dissecting the genomic complexity underlying medulloblastoma. Nature. 2012; 488:100–105. [PubMed: 22832583]

Junttila MR, de Sauvage FJ. Influence of tumour micro-environment heterogeneity on therapeutic response. Nature. 2013; 501:346–354. [PubMed: 24048067]

Kahn M. Can we safely target the WNT pathway? Nat Rev Drug Discov. 2014; 13:513–532. [PubMed: 24981364]

Kawauchi D, Robinson G, Uziel T, Gibson P, Rehg J, Gao C, Finkelstein D, Qu C, Pounds S, Ellison David W, et al. A Mouse Model of the Most Aggressive Subgroup of Human Medulloblastoma. Cancer Cell. 2012; 21:168–180. [PubMed: 22340591]

Kool M, Jones DT, Jager N, Northcott PA, Pugh TJ, Hovestadt V, Piro RM, Esparza LA, Markant SL, Remke M, et al. Genome sequencing of SHH medulloblastoma predicts genotype-related response to smoothened inhibition. Cancer Cell. 2014; 25:393–405. [PubMed: 24651015]

Logan CY, Nusse R. THE WNT SIGNALING PATHWAY IN DEVELOPMENT AND DISEASE. Annual Review of Cell and Developmental Biology. 2004; 20:781–810.

Marx V. Cancer: A most exceptional response. Nature. 2015; 520:389–393. [PubMed: 25877204]

Mohankumar KM, Currle DS, White E, Boulos N, Dapper J, Eden C, Nimmervoll B, Thiruvenkatam R, Connelly M, Kranenburg TA, et al. An in vivo screen identifies ependymoma oncogenes and tumor-suppressor genes. Nat Genet. 2015; 47:878–887. [PubMed: 26075792]

Muldoon LL, Soussain C, Jahnke K, Johanson C, Siegal T, Smith QR, Hall WA, Hynynen K, Senter PD, Peereboom DM, Neuwelt EA. Chemotherapy delivery issues in central nervous system malignancy: a reality check. Journal of clinical oncology : official journal of the American Society of Clinical Oncology. 2007; 25:2295–2305. [PubMed: 17538176]

Northcott PA, Jones DTW, Kool M, Robinson GW, Gilbertson RJ, Cho YJ, Pomeroy SL, Korshunov A, Lichter P, Taylor MD, Pfister SM. Medulloblastomics: the end of the beginning. Nat Rev Cancer. 2012a; 12:818–834. [PubMed: 23175120]

Northcott PA, Korshunov A, Witt H, Hielscher T, Eberhart CG, Mack S, Bouffet E, Clifford SC, Hawkins CE, French P, et al. Medulloblastoma Comprises Four Distinct Molecular Variants. Journal of Clinical Oncology. 2011; 29:1408–1414. [PubMed: 20823417]

Northcott PA, Shih DJH, Peacock J, Garzia L, Sorana Morrissy A, Zichner T, Stutz AM, Korshunov A, Reimand J, Schumacher SE, et al. Subgroup-specific structural variation across 1,000 medulloblastoma genomes. Nature. 2012b; 488:49–56. [PubMed: 22832581]

Oliver TG, Read TA, Kessler JD, Mehmeti A, Wells JF, Huynh TT, Lin SM, Wechsler-Reya RJ. Loss of patched and disruption of granule cell development in a pre-neoplastic stage of medulloblastoma. Development. 2005; 132:2425–2439. [PubMed: 15843415]

Parrish KE, Sarkaria JN, Elmquist WF. Improving drug delivery to primary and metastatic brain tumors: strategies to overcome the blood-brain barrier. Clin Pharmacol Ther. 2015; 97:336–346. [PubMed: 25669487]

Perreault S, Ramaswamy V, Achrol AS, Chao K, Liu TT, Shih D, Remke M, Schubert S, Bouffet E, Fisher PG, et al. MRI Surrogates for Molecular Subgroups of Medulloblastoma. American Journal of Neuroradiology. 2014; 35:1263–1269. [PubMed: 24831600]

Pugh TJ, Weeraratne SD, Archer TC, Pomeranz Krummel DA, Auclair D, Bochicchio J, Carneiro MO, Carter SL, Cibulskis K, Erlich RL, et al. Medulloblastoma exome sequencing uncovers subtype-specific somatic mutations. Nature. 2012; 488:106–110. [PubMed: 22820256]

Pyonteck SM, Akkari L, Schuhmacher AJ, Bowman RL, Sevenich L, Quail DF, Olson OC, Quick ML, Huse JT, Teijeiro V, et al. CSF-1R inhibition alters macrophage polarization and blocks glioma progression. Nat Med. 2013; 19:1264–1272. [PubMed: 24056773]

Reis-Filho JS, Pusztai L. Gene expression profiling in breast cancer: classification, prognostication, and prediction. The Lancet. 2011; 378:1812–1823.

Reis M, Czupalla CJ, Ziegler N, Devraj K, Zinke J, Seidel S, Heck R, Thom S, Macas J, Bockamp E, et al. Endothelial Wnt/β-catenin signaling inhibits glioma angiogenesis and normalizes tumor blood vessels by inducing PDGF-B expression. The Journal of Experimental Medicine. 2012; 209:1611–1627. [PubMed: 22908324]

Roberts KG, Mullighan CG. Genomics in acute lymphoblastic leukaemia: insights and treatment implications. Nat Rev Clin Oncol. 2015; 12:344–357. [PubMed: 25781572]

Robinson G, Parker M, Kranenburg TA, Lu C, Chen X, Ding L, Phoenix TN, Hedlund E, Wei L, Zhu X, et al. Novel mutations target distinct subgroups of medulloblastoma. Nature. 2012; 488:43–48. [PubMed: 22722829]

Schinkel AH, Wagenaar E, Mol CA, van Deemter L. P-glycoprotein in the blood-brain barrier of mice influences the brain penetration and pharmacological activity of many drugs. The Journal of clinical investigation. 1996; 97:2517–2524. [PubMed: 8647944]

Soda M, Choi YL, Enomoto M, Takada S, Yamashita Y, Ishikawa S, Fujiwara S-i, Watanabe H, Kurashina K, Hatanaka H, et al. Identification of the transforming EML4-ALK fusion gene in non-small-cell lung cancer. Nature. 2007; 448:561–566. [PubMed: 17625570]

Solomon BJ, Mok T, Kim DW, Wu YL, Nakagawa K, Mekhail T, Felip E, Cappuzzo F, Paolini J, Usari T, et al. First-Line Crizotinib versus Chemotherapy in ALK-Positive Lung Cancer. New England Journal of Medicine. 2014; 371:2167–2177. [PubMed: 25470694]

Spranger S, Bao R, Gajewski TF. Melanoma-intrinsic [bgr]-catenin signalling prevents anti-tumour immunity. Nature. 2015; 523:231–235. [PubMed: 25970248]

Stenman JM, Rajagopal J, Carroll TJ, Ishibashi M, McMahon J, McMahon AP. Canonical Wnt signaling regulates organ-specific assembly and differentiation of CNS vasculature. Science. 2008; 322:1247–1250. [PubMed: 19023080]

Thompson MC, Fuller C, Hogg TL, Dalton J, Finkelstein D, Lau CC, Chintagumpala M, Adesina A, Ashley DM, Kellie SJ, et al. Genomics identifies medulloblastoma subgroups that are enriched for specific genetic alterations. J Clin Oncol. 2006; 24:1924–1931. [PubMed: 16567768]

Uziel T, Zindy F, Xie S, Lee Y, Forget A, Magdaleno S, Rehg JE, Calabrese C, Solecki D, Eberhart CG, et al. The tumor suppressors Ink4c and p53 collaborate independently with Patched to suppress medulloblastoma formation. Genes Dev. 2005; 19:2656–2667. [PubMed: 16260494]

Vallon M, Chang J, Zhang H, Kuo CJ. Developmental and pathological angiogenesis in the central nervous system. Cellular and molecular life sciences : CMLS. 2014; 71:3489–3506. [PubMed: 24760128]

Verstappen CC, Koeppen S, Heimans JJ, Huijgens PC, Scheulen ME, Strumberg D, Kiburg B, Postma TJ. Dose-related vincristine-induced peripheral neuropathy with unexpected off-therapy worsening. Neurology. 2005; 64:1076–1077. [PubMed: 15781834]

Wang F, Zhou F, Kruh GD, Gallo JM. Influence of blood-brain barrier efflux pumps on the distribution of vincristine in brain and brain tumors. Neuro-oncology. 2010; 12:1043–1049. [PubMed: 20501632]

Yang ZJ, Ellis T, Markant SL, Read TA, Kessler JD, Bourboulas M, Schuller U, Machold R, Fishell G, Rowitch DH, et al. Medulloblastoma can be initiated by deletion of Patched in lineage-restricted progenitors or stem cells. Cancer cell. 2008; 14:135–145. [PubMed: 18691548]

Ye X, Wang Y, Cahill H, Yu M, Badea TC, Smallwood PM, Peachey NS, Nathans J. Norrin, frizzled-4, and Lrp5 signaling in endothelial cells controls a genetic program for retinal vascularization. Cell. 2009; 139:285–298. [PubMed: 19837032]

Yuen TJ, Silbereis JC, Griveau A, Chang SM, Daneman R, Fancy SP, Zahed H, Maltepe E, Rowitch DH. Oligodendrocyte-encoded HIF function couples postnatal myelination and white matter angiogenesis. Cell. 2014; 158:383–396. [PubMed: 25018103]

Zhou Y, Wang Y, Tischfield M, Williams J, Smallwood PM, Rattner A, Taketo MM, Nathans J. Canonical WNT signaling components in vascular development and barrier formation. The Journal of clinical investigation. 2014; 124:3825–3846. [PubMed: 25083995]

SIGNIFICANCE

Some cancers respond remarkably well to treatment. Better understanding of this treatment sensitivity could identify more effective therapies for less curable tumours. With this in mind, studies have focused on tumour cell intrinsic determinants of treatment response but the role of the microenvironment is less well understood. We show that the balance of agonistic and antagonistic WNT-signals from medulloblastoma cells in vivo, dictates whether tumour vessels form a functional blood brain barrier and therefore the degree to which medulloblastomas are exposed and respond to systemic chemotherapy. Because this tumour-endothelium WNT-signalling axis can be manipulated, pharmacological interventions might be used to disrupt the blood brain barrier in less curable brain tumours, increasing their exposure and response to chemotherapy.

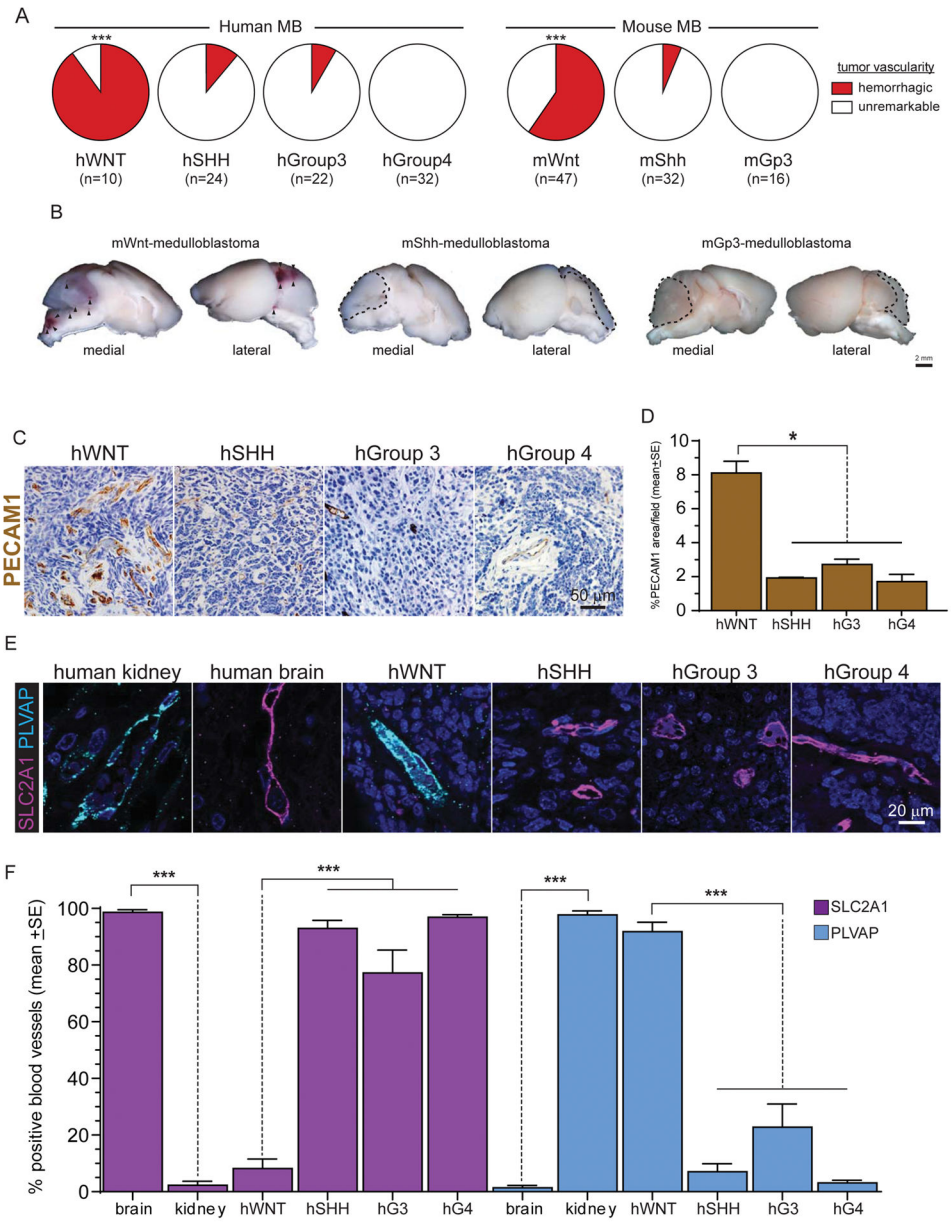

Figure 1. Human and mouse medulloblastoma vessel phenotype

A. Frequency of intra-operative haemorrhages detected in human and mouse medulloblastomas. **B.** Gross preparations of mouse medulloblastomas demonstrating numerous haemorrhages (arrows) in mWnt-medulloblastoma. Photomicrographs **(C)** and quantification **(D)** of PECAM1 immunohistochemical staining of human medulloblastomas. Co-immunofluorescence **(E)** and quantification **(F)** of SLC2A1 and PLVAP expression in human kidney, brain and medulloblastoma. *=P<0.05, ***=P<0.0005, Mann-Whitney. See also Figure S1.

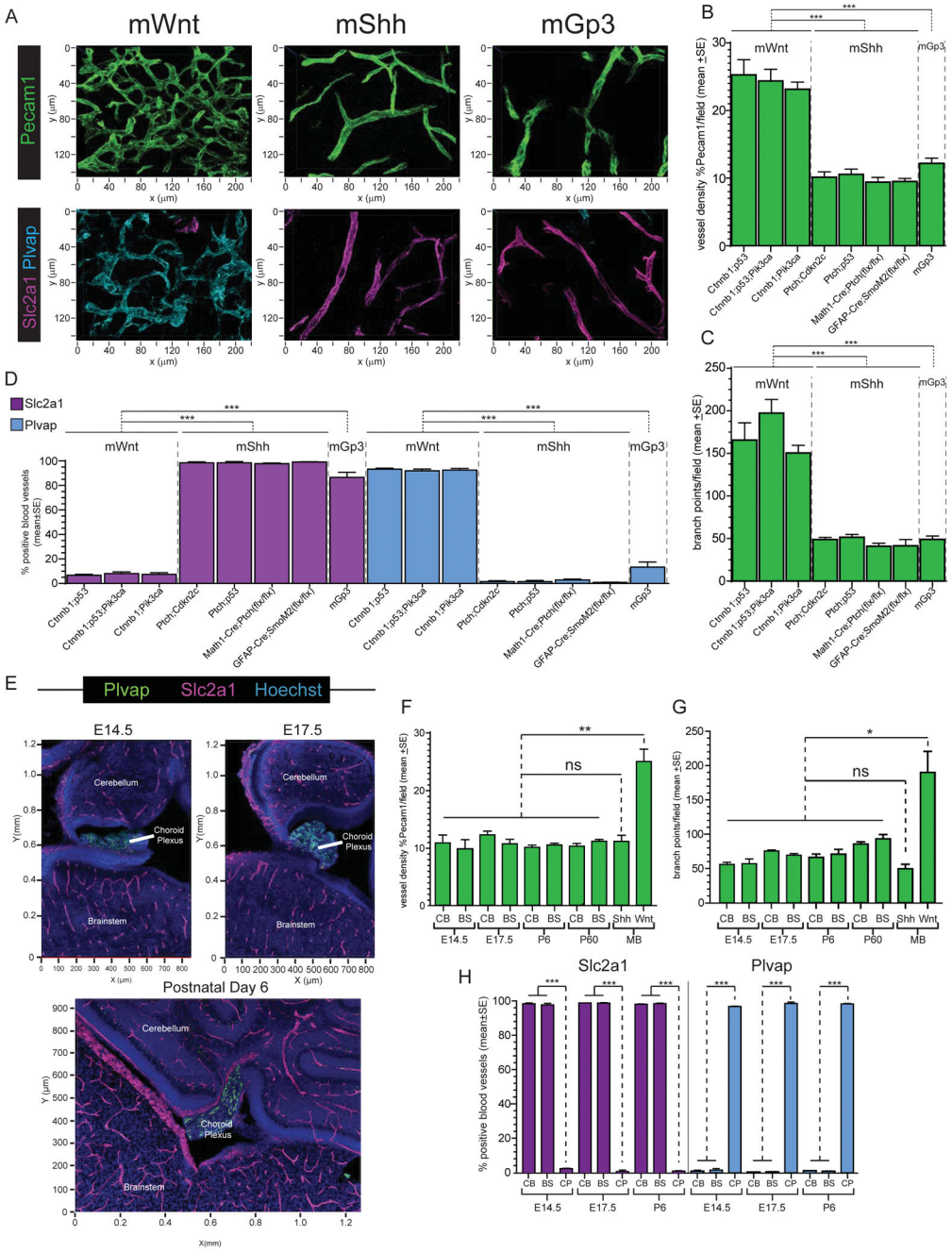

Figure 2. BBB immunophenotype in mouse medulloblastoma and developing hindbrain

A. Confocal immunofluorescence of Pecam1 (top) and co-immunofluorescence of Slc2a1 and Plvap (bottom) in mWnt-, mShh, and mGroup 3-medulloblastomas. Quantification of tumour vessel density **(B)**, tortuosity **(C)**, and Slc2a1/Plvap expression **(D)** in eight variant models of mWnt-, mShh, and mGroup 3-medulloblastoma. **E.** Co-immunofluorescence of Slc2a1 and Plvap in developing mouse hindbrain. Quantification of vessel density **(F)**, tortuosity **(G)**, and Slc2a1/Plvap expression **(H)** in developing mouse cerebellum (CB),

brainstem (BS) and choroid plexus (CP) relative to mWnt- and mShh-medulloblastomas (MB). *=P<0.05, **=P<0.005, ***=P<0.0005, Mann-Whitney. See also Figure S2.

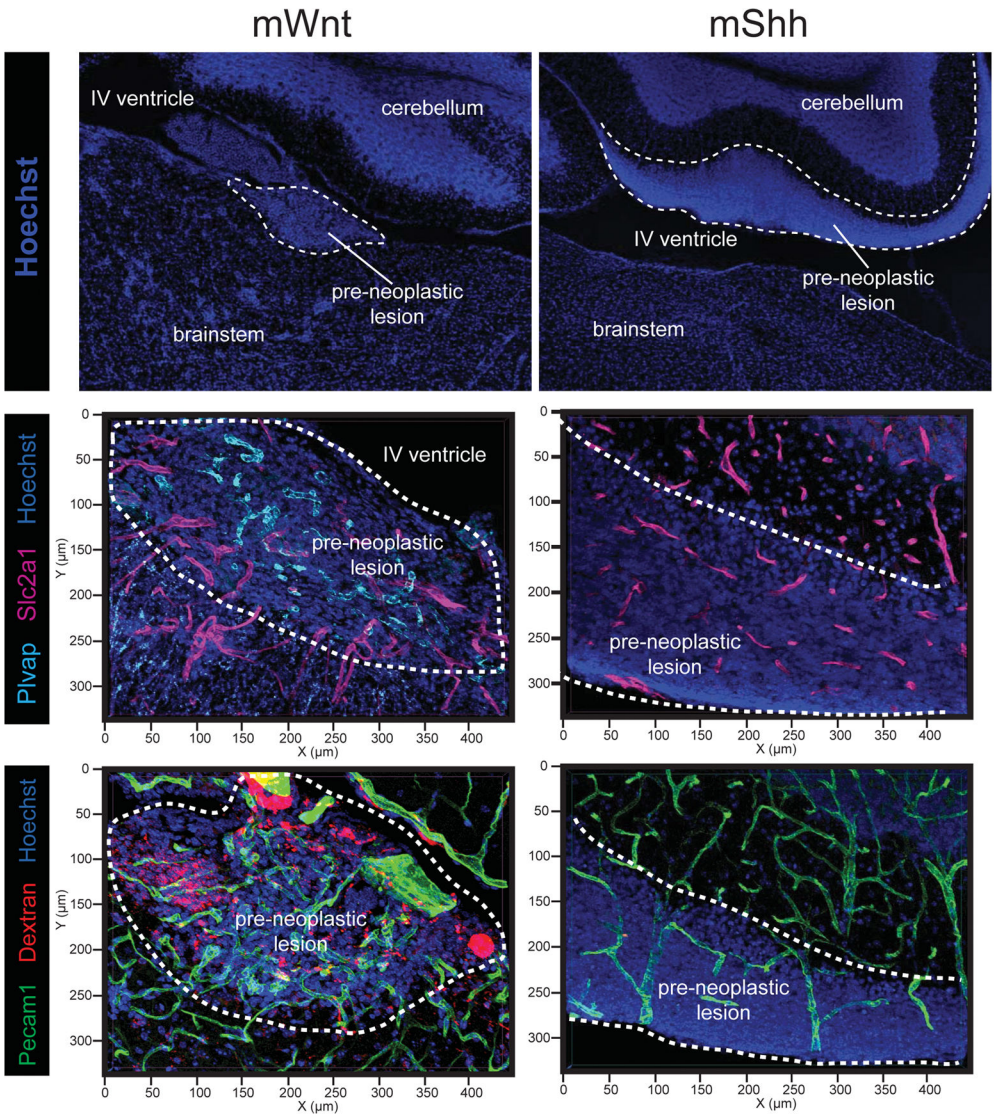

Figure 3. BBB immunophenotype and porosity in early hyperplasic precursor lesions of mWnt- and mShh-medulloblastoma

Top: Hoechst staining illustrating the anatomy and location of lesions in the developing hindbrain. Middle: co-immunofluorescence of Slc2a1 and Plvap in precursor lesions of mWnt- and mShh-medulloblastoma. Bottom: Pecam31 immunofluorescence and TMR-dextran autoflourescence demonstrating leakage of dextran into mWnt- but not mShh-medulloblastoma precursor lesions.

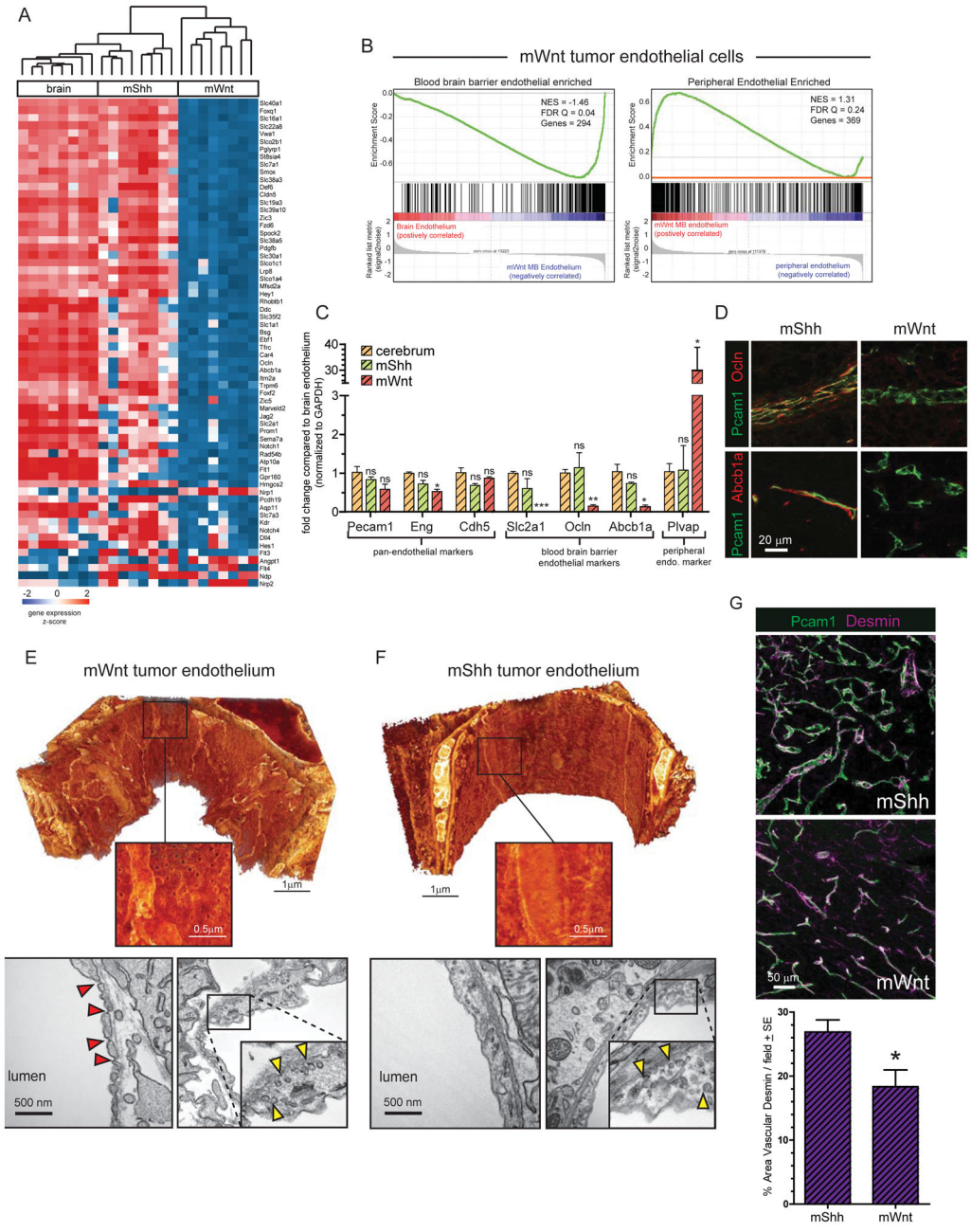

Figure 4. Molecular and ultrastructural phenotype of mWnt- and mShh-medulloblastoma endothelium

A. Unsupervised hierarchical clustering of BBB endothelial specific gene expression in endothelial cells isolated from mWnt- and mShh-medulloblastoma and normal brain. **B**. Gene Set Enrichment Analyses of BBB endothelium enriched (left) and peripheral endothelium enriched gene expression in mWnt-medulloblastoma endothelial cells reporting normalized enrichment score (NES) and the false discovery rate (FDR) Q value. **C.** Reverse-transcription quantitative polymerase chain reaction analyses of endothelial specific gene expression in endothelial cells isolated from normal brain, mWnt- and mShh-medulloblastoma. **D.** co-immunofluorescence of Pecam1 and Abcb1a or Ocln expression in

mWnt- and mShh-medulloblastoma endothelium. Electron microscopy (EM) of endothelium in mWnt- (**E)** and mShh-medulloblastoma **(F)**. In both E and top=3D scanning EM, bottom=transmission EM. View is from the interior of the vessel, bright objects are mitochondria. Note regular fenestrations in mWnt-medulloblastomas on 3D scanning EM. Red arrows=pores, yellow arrows=vesicles. **G.** Co-immunofluorescence (top) and quantification (bottom) of Desmin and Pecam31 expression in mWnt- and mShh-medulloblastoma. *=P<0.05, **=P<0.005, ***=P<0.0005, Mann-Whitney.

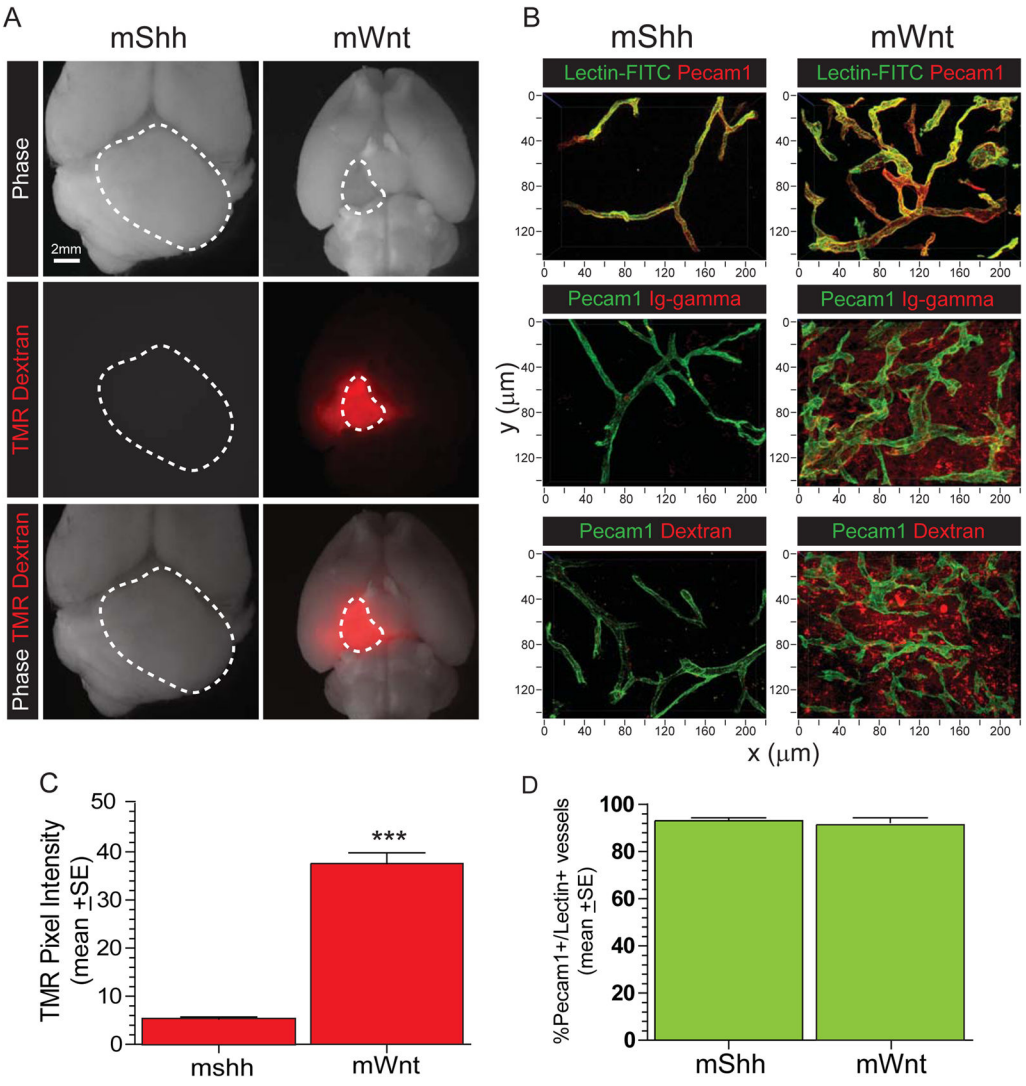

Figure 5. BBB function in mWnt- and mShh-medulloblastoma

A. Autofluorescence of TMR-Dextran in *ex vivo* whole brain preparations of mice harbouring mWnt- or mShh-medulloblastoma. Dotted lines demarcate tumours. **B.** confocal microscopy of Pecam1 immunofluorescence and lectin-FITC autoflourescence (top), gamma-immunoglobulin coimmunofluorescence (middle); and TMR-dextran autoflourescence; (bottom). Quantification of TMR-dextran in tissue fluid **(C)** and lectin-FITC in vessels **(D)** in mWnt- and mShh-medulloblastomas. ***=P<0.0005, Mann-Whitney.

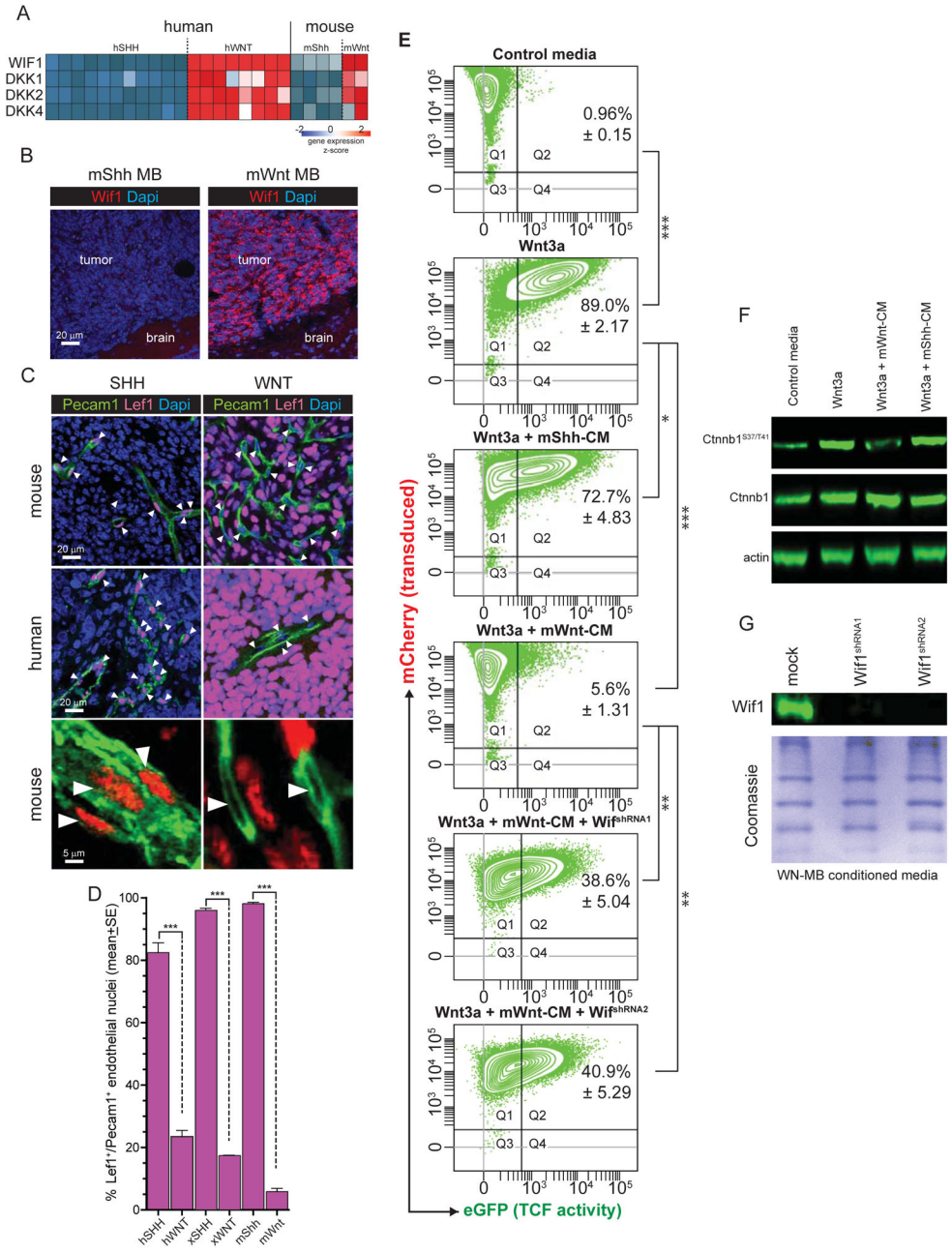

Figure 6. WNT-medulloblastoma paracrine signals silence WNT signalling in neighbouring cells

A. Heat map of mRNA expression of secreted WNT inhibitors by human and mouse medulloblastoma (source data Gibson et al., 2010). **B.** Immunofluorescence of Wif1 expression in mouse mWnt- and mShh-medulloblastoma. Co-immunofluorescence **(C)** and quantification **(D)** of Pecam1 and Lef1 expression in mouse mWnt- and mShh-medulloblastoma, arrows=nuclei. **E**. Fluorescence activated cell sorting plots quantifying TCF-reporter activity (x-axis) in TCF-reporter transduced cells (y-axis). Numbers in plots denote the %±SE of reporter transduced and activated cells. **F**. Western blots of total and phosphorylated Ctnnb1 in reporter cells shown in (E). **G.** Western blots of Wif1 in mWnt-

medulloblastoma cells transduced with Wif1-shRNAs. *=P<0.05, **=P<0.005, ***=P<0.0005, Mann-Whitney.

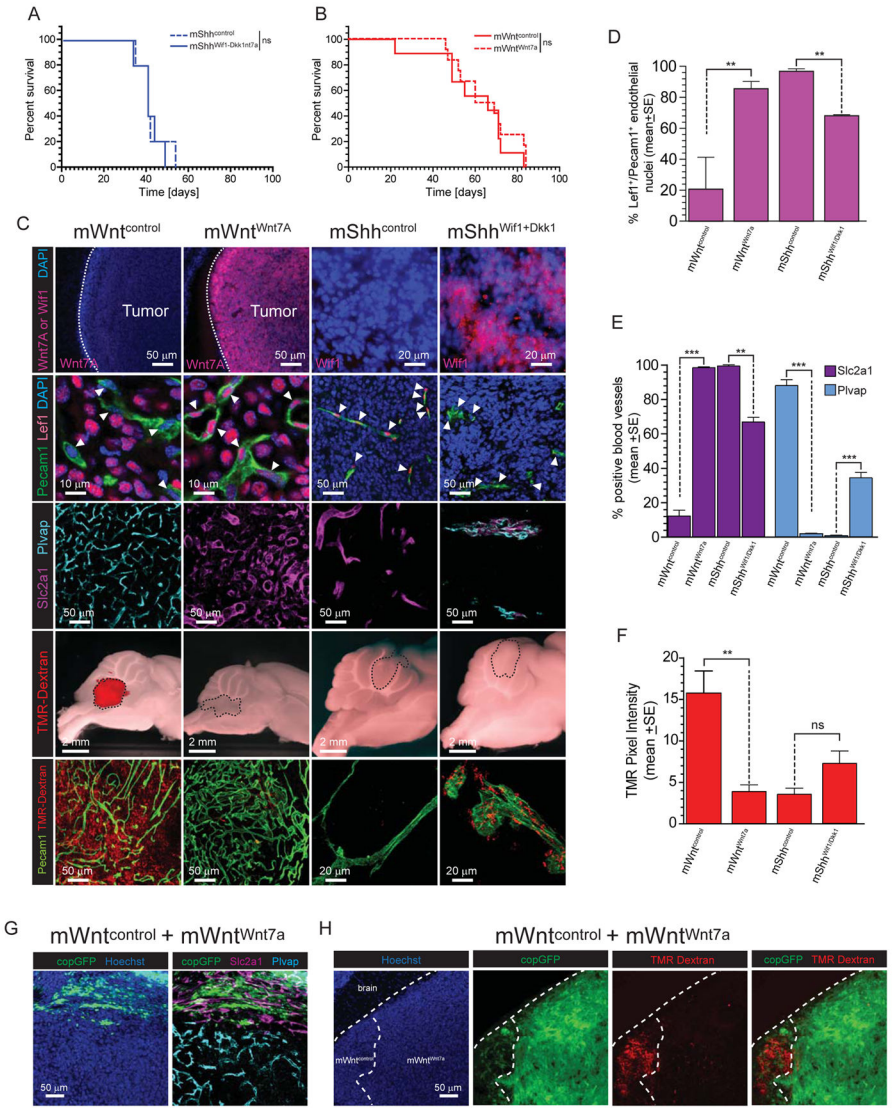

Figure 7. Medulloblastoma-endothelial paracrine signals can be manipulated in vivo

Kaplan-Meyer survival curves of **(A)** $mShh^{Wif1+Dkk1}$- or **(B)** or $mWnt^{Wnt1}$-medulloblastomas relative to controls. **C.** Immunofluorescence studies of the indicated proteins and TMR-dextran leakage in $mShh^{Wif1+Dkk1}$- and $mWnt^{Wnt1}$-medulloblastomas relative to controls. Quantification of $Lef1^+$ endothelial nuclei **(D)**, Slc2a1/Plvap expression **(E)** and TMR-dextran leakage **(F)** leakage in $mShh^{Wif1+Dkk1}$- and $mWnt^{Wnt1}$-medulloblastomas relative to controls. Slc2a1/Plvap expression (**G**) and TMR-dextran leakage **(H)** in admixed tumours of $mWnt^{Wnt1}$- and $mWnt^{control}$-medulloblastoma cells. **=P<0.005, ***=P<0.0005, Mann-Whitney. See also Figure S3.

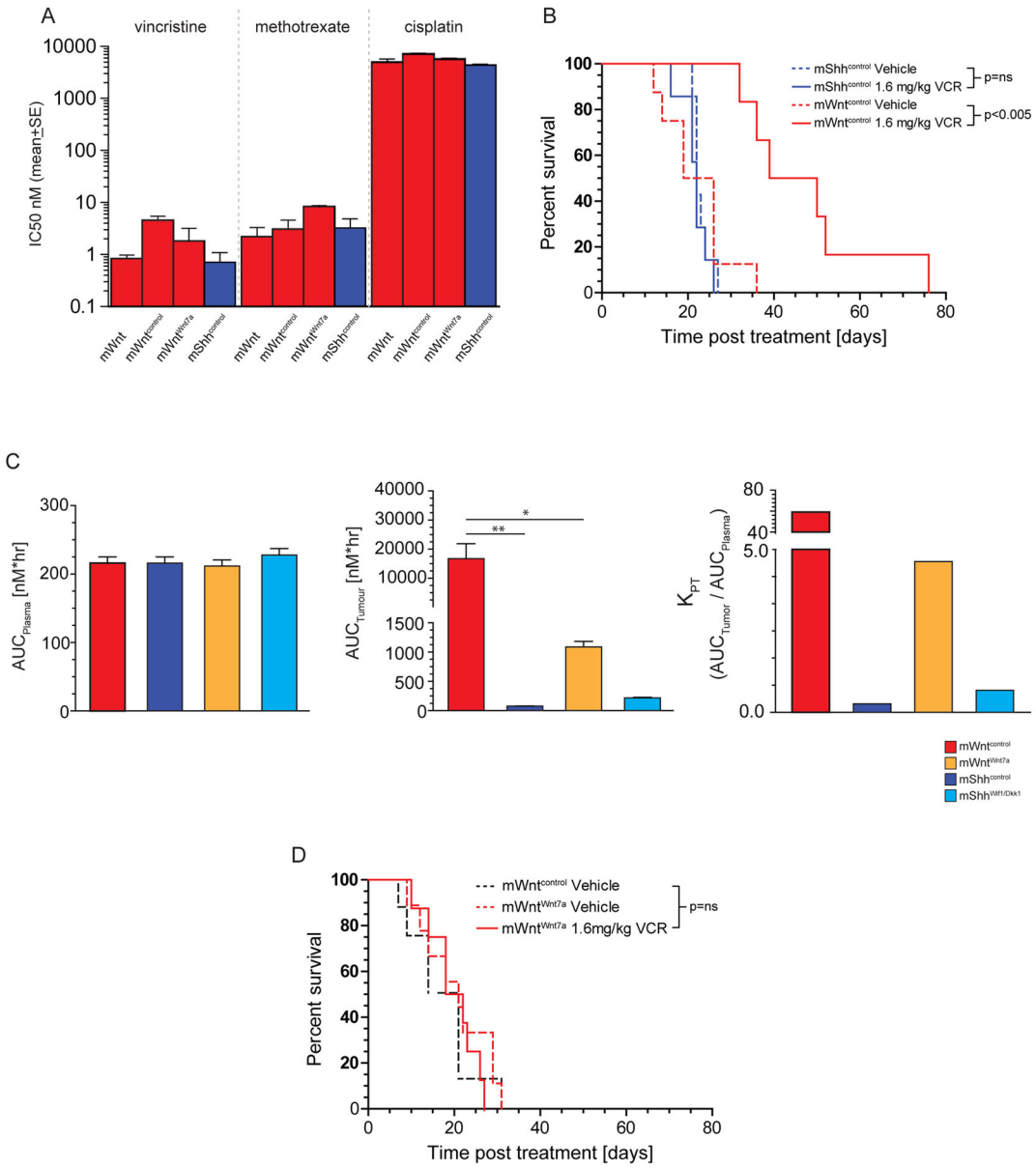

Figure 8. BBB function dictates medulloblastoma exposure and response to vincristine *in vivo*

A. Growth inhibition assays of mouse medulloblastoma cells following 72 hour exposure to the indicated drugs. **B.** Kaplan-Meyer survival curves of $mShh^{control}$ and $mWnt^{control}$-medulloblastomas to vincristine therapy. **C.** Vincristine area under the curve (AUC) plots for plasma (left), tumour tissue fluid (middle) and K_{PT} (right) in mice harbouring the indicated medulloblastomas. **D.** Kaplan-Meyer survival curves of $mWnt^{control}$- or $mWnt^{Wnt7a}$-medulloblastomas treated with vincristine therapy. *=P<0.05, **=P<0.005, Mann-Whitney.